Journal of Alloys and Compounds 920 (2022) 165563

Contents lists available at ScienceDirect

Journal of Alloys and Compounds

journal homepage: www.elsevier.com/locate/jalcom

Influence of stress-induced α" phase transformation on mechanical properties in metastable β type Ti-5Al-2.5Cr-5Mo-1Sn alloy

Kai Chen[a], Qunbo Fan[a,b,*], Jiahao Yao[a,b], Lin Yang[a,b], Shun Xu[a,b], Yu Gao[a], Wei Lei[a]

[a] National Key Laboratory of Science and Technology on Materials Under Shock and Impact, School of Materials Science and Engineering, Beijing Institute of Technology, Beijing 100081, China
[b] Beijing Institute of Technology Chongqing Innovation Center, Chongqing 401135, China

ARTICLE INFO

Article history:
Received 1 April 2022
Received in revised form 6 May 2022
Accepted 20 May 2022
Available online 23 May 2022

Keywords:
Titanium alloy
Phase transformation
Mechanical properties
Microstructure
Transmission electron microscopy

ABSTRACT

The stress-induced α" phase transformation in titanium alloys has received extensive attention due to its significant effect on mechanical properties. In this work, by adjusting the heat treatment process, the stress-induced α" phase transformation is activated in Ti-5Al-2.5Cr-5Mo-1Sn. The quasi-static tensile mechanical properties of the alloy under air-cooled and as-quenched states have been compared. Further, the morphology and orientation of the stress-induced α" phase and its interaction with dislocations are investigated by X-ray diffraction (XRD), optical microscope (OM), electron backscattered diffraction (EBSD) and transmission electron microscope (TEM) experiments. The value of average misorientation at the stress-induced α" bands region is larger than that in the β matrix, which indicates that the degree of plastic deformation in the stress-induced phase transformation region is higher. Therefore, the stress-induced α" phase exhibits a strong strain partitioning effect during the stretching process and improves the ductility of the material. The β/α" interface has a weak effect to hinder the dislocations, which results in low tensile strength of the alloy. This work can provide insight into the influence of stress-induced α" phase transformation on the mechanical properties of transformation induced plasticity (TRIP) type titanium alloys.

1. Introduction

The diversity of phase transformation types is the important characteristic of metastable β titanium alloys. With the increase of β phase stability, a series of structures such as α' martensite [1], α" martensite [2], ω phase [3] and twinning [4] may be formed during deformation, which significantly affects the mechanical properties of titanium alloys.

The α" phase transformation has attracted extensive attention because of its ability to produce high strain hardening rate [5] and low elastic modulus [6]. The α" phase in titanium alloys usually formed by the stress induction from the as-quenched metastable β phase. It is generally believed that the atomic shear process of β→α" phase transformation involves the shearing of $\{11\bar{2}\}_\beta$ planes in $< 111 >_\beta$ direction and shuffling of atoms on parallel adjacent $\{110\}_\beta$ planes in $< 110 >_\beta$ direction [7]. In previous studies, a series of titanium alloys with stress-induced α" phase transformation were designed by d-electron theory [8], such as Ti-12Mo [9], Ti-9Mo-6 W [10] and Ti-24 Nb-4Zr-8Sn [11]. These alloys undergo a transformation induced plasticity (TRIP) effect during stretching, which enables high elongation of the material. However, the alloys generally exhibit low yield strengths of 200 MPa ~ 500 MPa, which is believed to be a negative effect of stress-induced α" phase transformation. In response to this phenomenon, Ti-3Al-5Mo-7 V-3Cr [12] and Ti-12Mo-5Zr [13] alloys were developed to introduce $\{332\} < 113 >$ twins to improve the yield strength of the alloys. Besides, Gao [14] designed Ti-7Mo-3Cr by introducing athermal ω phase into the alloy, which suppressed the occurrence of stress-induced α" phase transformation during early stage of plastic deformation. This avoids the reduction in yield strength while taking advantage of the high strain hardening effect caused by the stress-induced phase transformation.

The above works reflect the significant effect of α" phase transformation on the mechanical properties of titanium alloys. On this basis, we explore the internal mechanism of the stress-induced α" phase transformation on the ductility and strength in Ti-5Al-2.5Cr-5Mo-1Sn titanium alloy.

* Corresponding author at: National Key Laboratory of Science and Technology on Materials Under Shock and Impact, School of Materials Science and Engineering, Beijing Institute of Technology, Beijing 100081, China.
E-mail address: fanqunbo@bit.edu.cn (Q. Fan).

https://doi.org/10.1016/j.jallcom.2022.165563
0925-8388/

Table 1
Measured chemical compositions of the alloy in wt%.

Elements	Ti	Al	Cr	Mo	Sn	C	N	O	H
Measured	Bal.	5.16	2.49	4.94	1.08	0.021	0.011	0.090	0.0069

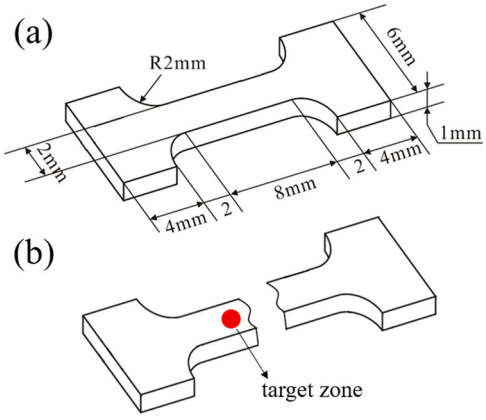

Fig. 1. Schematic diagram of the tensile specimen. (a) Dimensions of the tensile specimen. (b) Target zone for microstructural characterization.

2. Material and methods

The Ti-5Al-2.5Cr-5Mo-1Sn alloy in this work was cast via vacuum arc smelting for three times. The contents of metallic elements were analyzed via an inductively coupled plasma optical emission spectrometer (ICP-OES, Agilent 730), the O, N, H concentration were determined by an ONH-3000 analyzer, and the C concentration was determined by CS-3000 analyzer. The measured chemical compositions are listed in Table 1. The β transus temperature for this material is about 900 ℃. The ingot underwent homogenization at 1000 °C for 12 h, and was then forged at 800 °C, reaching a deformation of 75%. Finally, the forged samples were solution-treated at 930 °C for 30 min, and then cooled to room temperature by water quenching and air cooling.

The quasi-static tensile tests were carried out on an Instron 5565 system using a video extensometer at a nominal strain rate of 0.5×10^{-3} s^{-1}. The dimensions of the tensile specimen are shown in Fig. 1**a**. After tension, samples were processed from the gauge sections (the red circled zone in Fig. 1**b**) for subsequent X-ray diffraction (XRD), optical microscope (OM), electron backscattered diffraction (EBSD) and transmission electron microscope (TEM) observations.

The phase identification before and after tension were made by XRD analysis using a Bruker D8 Focus diffractometer with Cu-Ka radiation and operating at 40 kV and 40 mA. The spot size, exposure time, scan speed, and scan interval were set as 1 mm (diameter), 20 s, 2º/min, and 20º - 80º, respectively. An interaction volume of 7.85×10^6 μm^3 is achievable for the beam conditions employed in this study. The observation of stress-induced structures after tension was carried out on optical microscopy (LECO series Olympus PME-3) with a magnification of 100 ×. The EBSD maps were recorded under a voltage of 25 kV and current of 26 μA on field emission scanning electron microscope (JSM 7200 F). Prior to this process, the surface of specimen was mechanically polished, and then electrolytically polished in a $HClO_4$:$CH_3(CH_2)_3OH$:CH_3OH (6:34:60) solution at 30 V, and − 40 °C. The scan area was set as 1 mm × 1 mm for grain size statistics and 100 μm × 100 μm for the identification of stress-induced bands. The percentage of the initial indexed points is between

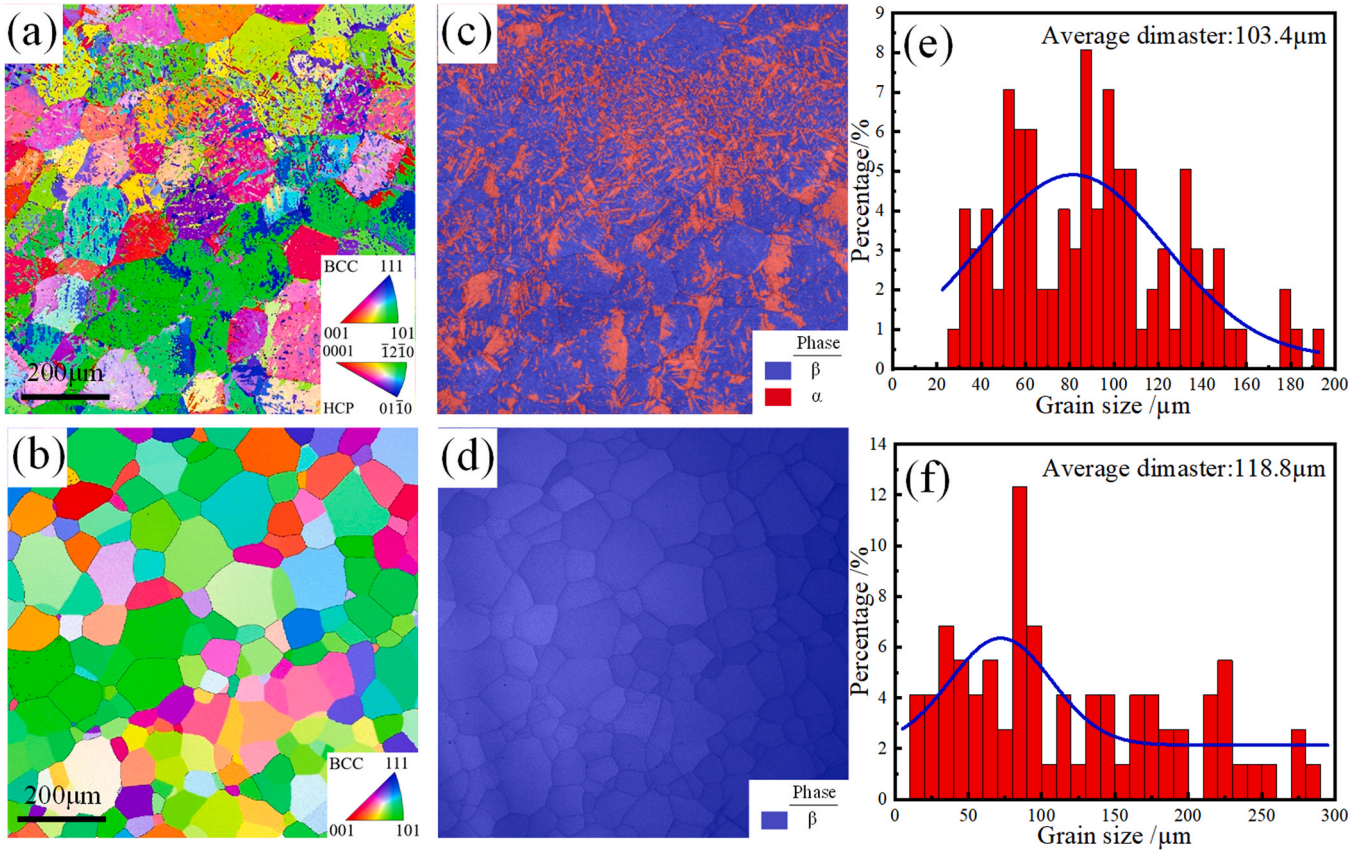

Fig. 2. EBSD analysis of the air-cooled and as-quenched alloys. (a),(b) IPF maps of the air-cooled and as-quenched alloys, respectively. (c),(d) Phase maps of the air-cooled and as-quenched alloys, respectively. (e),(f) Statistical histograms and distribution curves for the β grain sizes in (a) and (b), respectively.

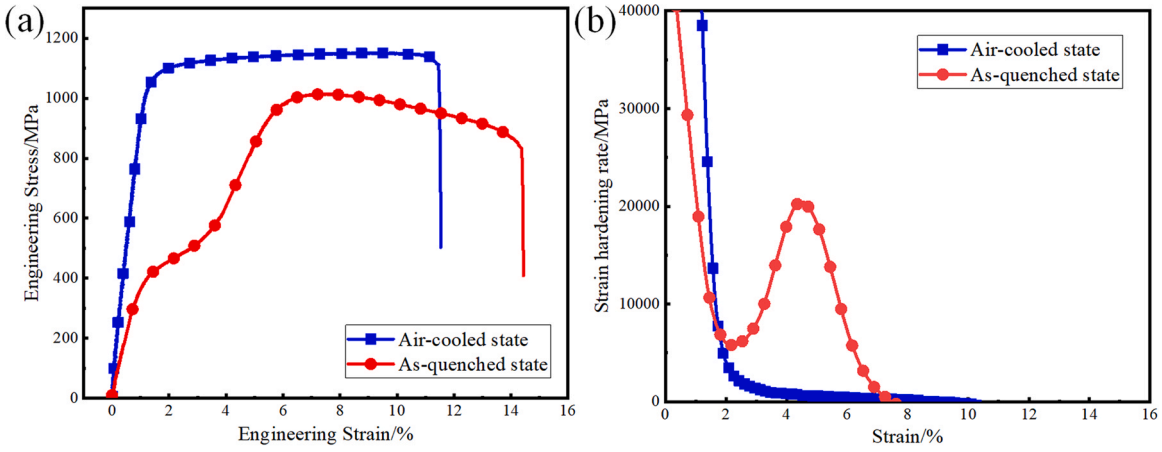

Fig. 3. Analysis of quasi-static tensile properties of air-cooled and as-quenched alloys. (a) Engineering stress-strain curves. (b) Strain hardening rate curves.

90% and 95%. After data cleaning using HKL's CHANNEL5 software, the indexed points proportion reached 100%. The EBSD inverse pole figure (IPF) map, band contrast (BC) map, phase map, and kernel average misorientation (KAM) map were obtained by HKL's CHANNEL5 and ATEX software. The TEM tests were performed under a Talos F200X transmission electron microscope equipped with a 200 kV electron gun. Samples were prepared by ion thinning method after grinding with SiC papers to a thickness of ~100 μm. The selected area electron diffraction (SAED) patterns and high resolution (HR) TEM images were analyzed using Digital Micrograph (GMS 3, Gatan, Munich, Germany) software.

3. Results and discussion

3.1. Microstructure and mechanical properties of air-cooled and as-quenched alloys

The materials are heat treated at 930 ℃ for 30 min, and then cooled to room temperature with air and water, respectively. After heat treatment, the air-cooled alloy consists of β and α phases (Fig. 2**a and c**). Under the condition of slow cooling, the α stabilizing elements Al and Sn and the β stabilizing elements Mo and Cr have enough time to diffuse, so that the α phase precipitates from the β phase to form a two-phase structure. In contrast, the as-quenched microstructure is composed of the single β phase (Fig. 2**b and d**). The metastable β phase is completely retained to room temperature under quenched conditions. Statistics on the measured β grain sizes and distribution curves fitted by Gaussian function are shown in Fig. 2**e-f**. The average β grain sizes of air-cooled and as-quenched alloy are 103.4 μm (standard deviation of 38.3) and 118.8 μm (standard deviation of 50.7) respectively, which are approximately equal. Previous studies showed that the size of β grains depends on the holding temperature and holding time above the β transus temperature [15]. The heat treatment processes in this work keep these two parameters constant. Therefore, the influence of the initial β grain size on the mechanical properties of the two heat treatments states can be excluded.

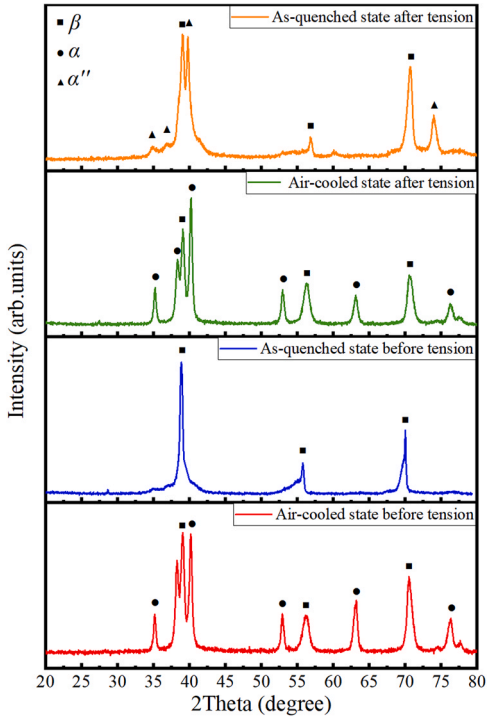

Fig. 4. XRD analysis of the air-cooled and as-quenched alloys.

The quasi-static stretching curves of the air-cooled and as-quenched alloys are shown in Fig. 3**a**. The yield strength, ultimate tensile strength and total elongation of the air-cooled alloy are ~1080 MPa, ~1150 MPa and 11.6%, respectively. In contrast, the yield strength, ultimate tensile strength and total elongation of the as-quenched alloy are ~380 MPa, ~1000 MPa and 14.2%, respectively. It is found that the yield strength and tensile strength of the as-quenched alloy are lower than those of the air-cooled alloy, while the ductility is improved. Fig. 3**b** shows the strain hardening rate curves of the two states. The air-cooled state shows a downward trend with strain accumulation, and gradually flattens during the plastic section (> 2%). However, the strain hardening rate of as-quenched state increases abnormally between 2% and 5% strains, and the maximum strain hardening rate reaches ~20 GPa. This phenomenon indicates that the phase transformation takes place in the as-quenched alloy during deformation.

3.2. Microstructure analysis of the alloys after tension

The XRD analysis of the two state alloys before and after tension are shown in Fig. 4. There is no change in the phase of the air-cooled alloy before and after tension, both of which are composed of α and β phases. However, the as-quenched alloy is composed of β phase before tension, and the diffraction peaks of α'' phase appear after tension, indicating that stress-induced α'' phase transformation occurs in this state during stretching process.

The fracture morphologies of the two states after tension are shown in Fig. 5. For the air-cooled alloy, the slip bands can be clearly observed at the fracture surface (Fig. 5**a**), indicating that its plastic

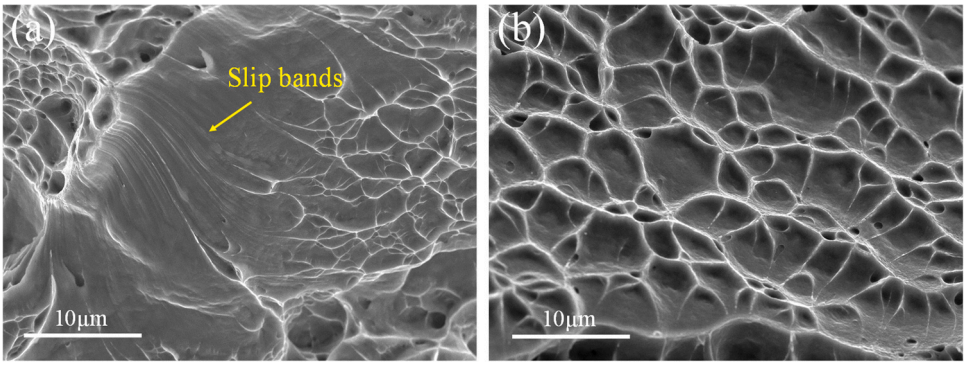

Fig. 5. The fracture morphologies of the air-cooled and as-quenched alloys after stretching. (a) Air-cooled state. (b) As-quenched state.

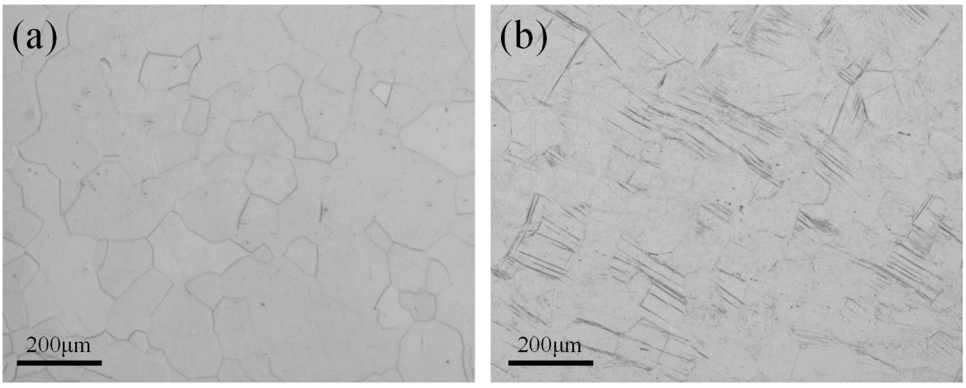

Fig. 6. Metallographic analysis of the as-quenched alloy before and after tension. (a) Before tension. (b) After tension.

deformation mode is controlled by dislocation slip. However, the fracture surface of the as-quenched sample has a large number of dimples with a diameter of ~4 μm (Fig. 5**b**). This proves that the fracture mode of the as-quenched alloy is ductile fracture [16], which contributes to its higher elongation.

3.3. Mechanisms analysis of the stress-induced α" phase transformation's influence on mechanical properties

Fig. 6**a** and 6**b** correspond to the metallographic microstructure of the as-quenched alloy before and after tension, respectively. By comparison, it is found that the stress-induced α" phase exhibits the morphology of bands. These bands are identified as an orthorhombic structure (space group: cmcm 63) by the EBSD IPF map (Fig. 7**a**). The body centered cubic (BCC) β phase and the orthorhombic α" phase are shown in red and blue respectively in the EBSD phase map (Fig. 7**b**). The KAM map shows that the localized misorientation angle distribution in the scanned area exhibits non-uniformity (Fig. 7**c**), reflecting the different degrees of plastic deformation among various microstructures. The ductility of titanium alloy composed of single β phase is usually low, which is due to the intergranular fracture caused by the concentration of strain at β grain boundaries. This phenomenon is also shown in Fig. 7**c**, the value of average misorientation at the β grain boundary is higher than that in the β grain interior. Be similar with the grain boundaries region, the stress-induced bands region also exhibits a high average misorientation value, which indicates that the degree of plastic deformation in this region is higher than that of β matrix [17,18]. Therefore, the formation of stress-induced α" phase during the stretching process plays a role in coordinating the strain. The higher strain accumulation in the bands avoids the strain concentration at the grain boundaries, thus promoting the ductility of the material.

The as-quenched samples after tension are further characterized by TEM. Bright-field (BF) image reveals the existence of parallel band structures in the β matrix with an average width of ~60 nm (Fig. 8**a**). The bands are identified as α" phase by the selected area electron diffraction (SAED) along the $[01\bar{1}]_{\beta}$ axis (Fig. 8**b**). Fig. 8**c** shows the high resolution (HR) TEM image at the interface of β/α". Combined with HRTEM image and SAED, the orientation relationship between β and α" phases can be judged as $[01\bar{1}]_{\beta}//[001]_{\alpha"}$, $[011]_{\beta}//[010]_{\alpha"}$ and $[100]_{\beta}//[100]_{\alpha"}$, as shown in diagram Fig. 8**d**. In addition, it is observed that the interface of β/α" exhibits the semi-coherent characteristic. The lattice misfit in the directions of $[001]_{\alpha"}$, $[010]_{\alpha"}$ and $[100]_{\alpha"}$ are calculated [19]:

$$\delta_{[001]} = |a_{\beta} - a_{\alpha"}|/a_{\beta},\ \delta_{[010]} = |\sqrt{2}\,b_{\beta} - b_{\alpha"}|/\sqrt{2}\,b_{\beta},\ \delta_{[100]} = |\sqrt{2}\,c_{\beta} - c_{\alpha"}|/\sqrt{2}\,c_{\beta} \quad (1)$$

Where $a_{\beta} = b_{\beta} = c_{\beta} = 0.328$ nm represent the lattice parameters of the β phase [20]; $a_{\alpha"} = 0.3166$ nm, $b_{\alpha"} = 0.4854$ nm and $c_{\alpha"} = 0.4652$ nm represent the lattice parameters of the α" phase [21].

The calculated lattice strains in the three directions are 3.5%, 4.7% and 0.3%, respectively, which conforms to the semi-coherent characteristic and is consistent with the experimental observation.

Compared with the air-cooled state, the as-quenched alloy exhibits a low yield strength of ~380 MPa. The stress-induced α" phase transformation occurring at a low stress produces the stress plateau, which manifests as macroscopically yielding of the specimen [22]. Previous studies have shown that the trigger stress for stress-induced α" phase transformation fluctuates between 200 MPa ~ 500 MPa, which is affected by the heat treatment process [23], the grain size of matrix β phase [24], the strain rate [25,26], and the composition of alloying elements [27]. Therefore, the low trigger stress of β→α" phase transformation in the as-quenched alloy results

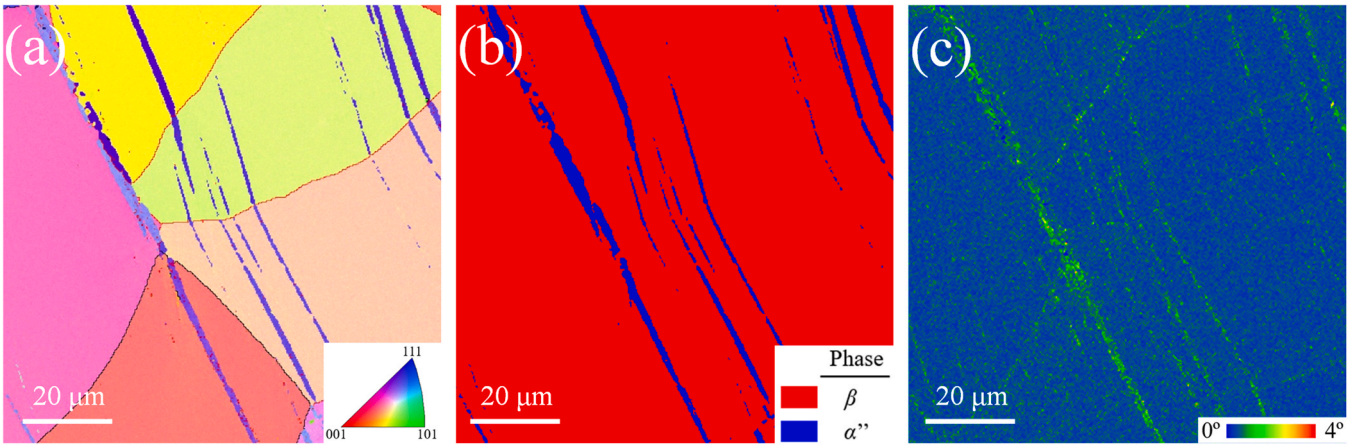

Fig. 7. EBSD analysis of the bands structure after tension. (a) IPF map. (b) Phase map. (c) KAM map.

in its low yield strength. In addition, the ultimate tensile strength of the as-quenched state is also found to be lower than that of the air-cooled state. According to the Hall-Petch formula [28,29], within a certain range, the smaller the grain size of the material, the higher the strength. Given that the β grain sizes of the two states are very close, the effect of grain refinement on the strength of the alloy can be ruled out. Therefore, the difference in strength between the two states attributes to the effects of the stress-induced α'' phase in as-quenched alloy and the α phase in air-cooled alloy. It is generally believed that the improvement of the strength of metallic materials is related to the dislocation mean free path. The relationship between the material flow stress increment $\Delta\sigma_l$ and the dislocation mean free path Λ is shown as follows [30]:

$$\Delta\sigma_l = nMGb/\Lambda \quad (2)$$

Where n represents the maximum number of dislocations accumulated at the grain boundary on a specific slip plane; M represents the Taylor factor; G is the alloy shear modulus; and b represents the magnitude of the Burgers vector.

The nanoscale secondary α phase can be formed from the β phase by aging heat treatment, which can hinder the movement of

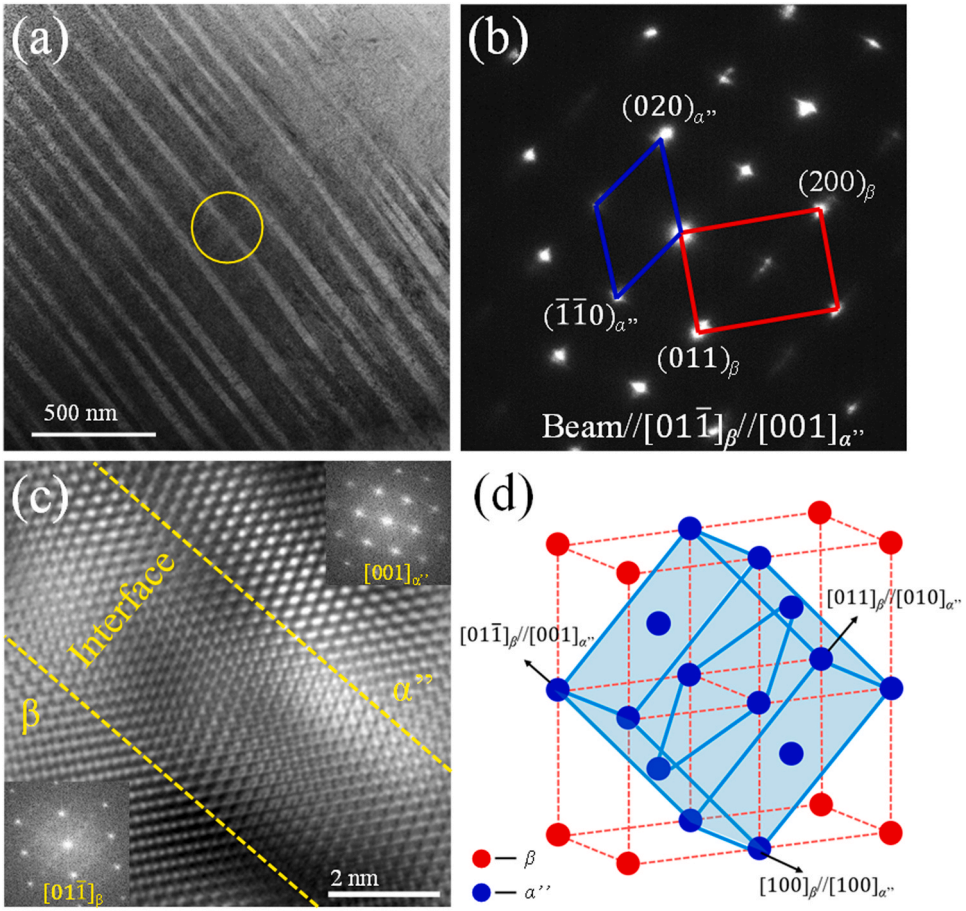

Fig. 8. TEM analysis of the bands structure. (a) TEM BF image. (b) SAED pattern along the $[01\bar{1}]_\beta$ zone axis recorded from the circled area in (a). (c) The HRTEM image of the β/α'' interface. (d) Schematic diagram of the orientation relationship between the β and α'' phases.

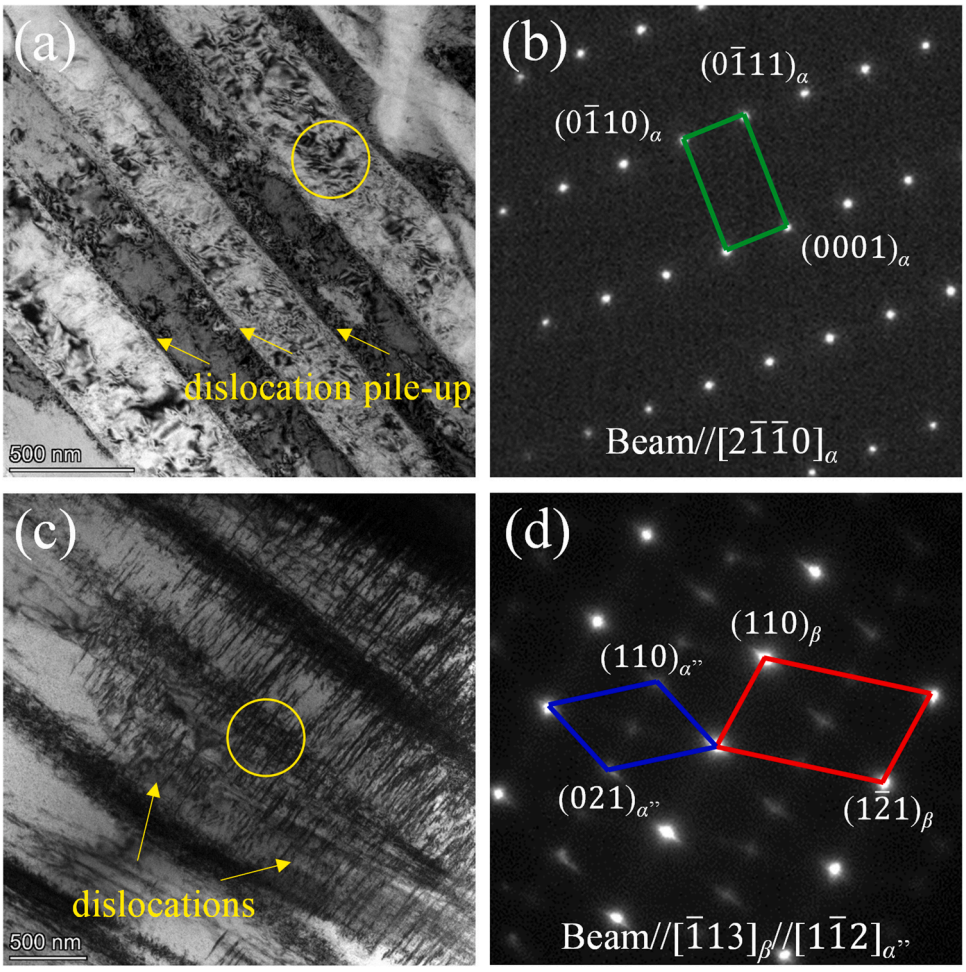

Fig. 9. Dislocations analysis for the air-cooled and as-quenched alloys after tension. (a) TEM BF image of the air-cooled alloy. (b) SAED pattern recorded from the circled area in (a). (c) TEM BF image of the as-quenched alloy. (d) SAED pattern recorded from the circled area in (c).

dislocations, thereby shortening the mean free path of dislocations and improving the tensile strength [31–33]. In order to explore the interaction between the second phase and dislocations in the two states alloys, the morphologies of the dislocations near the α phase and the α" bands are observed by TEM. Fig. 9**a** shows the TEM BF image of the air-cooled alloy. SAED pattern recorded from the circled area proves that the band in Fig. 9**a** is the hexagonal close-packed (HCP) α phase (Fig. 9**b**). It is observed that dislocations are hindered at the β/α interface to form dislocation pile-ups. As a comparison, the TEM BF image of the as-quenched alloy is shown in Fig. 9**c**, the bands structure in the figure is retrieved as α" phase, and its orientation relationship with β phase is $[\bar{1}13]_\beta//[1\bar{1}2]_{\alpha''}$ (Fig. 9**d**). It is observed that dislocations can propagate directly through the bands without being hindered by the β/α" phase interface. Because the interface between α" and β phases is semi-coherent with low distortion, the difficulty of dislocation slip at the interface is reduced. Therefore, α" phase has a weak hindering effect on dislocations. The dislocation mean free path of as-quenched alloy is obviously higher than that of the air-cooled alloy, which is the reason why the ultimate tensile strength of as-quenched alloy with α" phase transformation is generally lower.

4. Conclusion

In this paper, the mechanism of the effect of stress-induced α" phase transformation on the strength and ductility of the material is explored in Ti-5Al-2.5Cr-5Mo-1Sn alloy. Due to the activation of stress-induced α" phase transformation, the alloy under as-quenched state exhibits lower yield strength and tensile strength, but higher total elongation than that of air-cooled state. The stress-induced α" bands exhibit a strong strain partitioning effect during deformation. This avoids the concentration of strain in the original large β grains, thereby promoting the improvement of alloy ductility. The interface between α" and β phases is semi-coherent. Compared with the α/β interface, the α"/β interface exhibits a weaker effect to hinder dislocations movement, which is the reason for the low tensile strength of the as-quenched alloy.

CRediT authorship contribution statement

Kai Chen: Methodology, Investigation, Formal analysis, Writing. **Qunbo Fan**: Methodology, Supervision, Funding acquisition. **Jiahao Yao**: Supervision, Review, Editing. **Lin Yang**: Supervision, Review, Editing. **Shun Xu**: Review, Editing, Funding acquisition, Supervision. **Yu Gao**: Supervision, Review, Editing. **Wei Lei**: Supervision, Review, Editing.

Declaration of Competing Interest

The authors declare that they have no known competing financial interests or personal relationships that could have appeared to influence the work reported in this paper.

Acknowledgements

The authors are grateful to the financial support from the Natural Science Foundation of China (Grant No. 51901102).

References

[1] Y. Fu, W. Xiao, D. Kent, M.S. Dargusch, J. Wang, X. Zhao, C. Ma, Ultrahigh strain hardening in a transformation-induced plasticity and twinning-induced plasticity titanium alloy, Scr. Mater. 187 (2020) 285–290.
[2] J.F. Xiao, X.K. Shang, J.H. Hou, Y. Li, B.B. He, Role of stress-induced martensite on damage behavior in a metastable titanium alloy, Int. J. Plast. 146 (2021) 103103.
[3] H. Liu, M. Niinomi, M. Nakai, K. Cho, H. Fujii, Deformation-induced ω-phase transformation in a β-type titanium alloy during tensile deformation, Scr. Mater. 130 (2017) 27–31.
[4] L. Ren, W. Xiao, D. Kent, M. Wan, C. Ma, L. Zhou, Simultaneously enhanced strength and ductility in a metastable β-Ti alloy by stress-induced hierarchical twin structure, Scr. Mater. 184 (2020) 6–11.
[5] X. Ma, F. Li, X. Fang, Z. Li, Z. Sun, J. Hou, J. Cao, Effect of strain reversal on the stress-induced martensitic transformation and tensile properties of a metastable β titanium alloy, J. Alloy. Compd. 784 (2019) 111–116.
[6] K. Li, M. Li, Y. Zhao, W. Shan, Y. Cao, D. Guo, Achieving ultralow elastic modulus in TiNi alloy by controlling nanoscale martensite phase, Mater. Lett. 233 (2018) 282–285.
[7] M. Bönisch, T. Waitz, M. Calin, W. Skrotzki, J. Eckert, Tailoring the Bain strain of martensitic transformations in Ti-Nb alloys by controlling the Nb content, Int. J. Plast. 85 (2016) 190–202.
[8] M. Morinaga, N. Yukawa, H. Adachi, Theory of the d electrons alloy design, J. Iron Steel Inst. 71 (1985) 1441–1451.
[9] M. Marteleur, F. Sun, T. Gloriant, P. Vermaut, P.J. Jacques, F. Prima, On the design of new β-metastable titanium alloys with improved work hardening rate thanks to simultaneous TRIP and TWIP effects, Scr. Mater. 66 (2012) 749–752.
[10] F. Sun, J. Zhang, M. Marteleur, C. Brozek, F. Prima, A new titanium alloy with a combination of high strength, high strain hardening and improved ductility, Scr. Mater. 94 (2015) 17–20.
[11] T. Yao, K. Du, H. Wang, Z. Huang, C. Li, L. Li, Y. Hao, R. Yang, H. Ye, In situ scanning and transmission electron microscopy investigation on plastic deformation in a metastable b titanium alloy, Acta Mater. 133 (2017) 21–29.
[12] S. Sadeghpour, S.M. Abbasi, M. Morakabati, A. Kisko, L.P. Karjalainen, D.A. Porter, A new multi-element beta titanium alloy with a high yield strength exhibiting transformation and twinning induced plasticity effects, Scr. Mater. 145 (2018) 104–108.
[13] J. Zhang, J. Li, G. Chen, L. Liu, Z. Chen, Q. Meng, B. Shen, F. Sun, F. Prima, Fabrication and characterization of a novel β metastable Ti-Mo-Zr alloy with large ductility and improved yield strength, Mater. Charact. 139 (2018) 421–427.
[14] J. Gao, Y. Huang, D. Guan, A.J. Knowles, L. Ma, D. Dye, W.M. Rainforth, Deformation mechanisms in a metastable beta titanium twinning induced plasticity alloy with high yield strength and high strain hardening rate, Acta Mater. 152 (2018) 301–314.
[15] J. Wang, W. Xiao, Y. Fu, L. Ren, C. Ma, Dependence of mechanical behavior on grain size of metastable Ti-Nb-O titanium alloy, 2021.
[16] J. Wang, Y. Zhao, W. Zhou, Q. Zhao, S. Huang, W. Zeng, In-situ investigation on tensile deformation and fracture behaviors of a new metastable β titanium alloy, Mater. Sci. Eng. A 799 (2021) 140187.
[17] Y. Takayama, J.A. Szpunar, H. Kato, Analysis of intragranular misorientation related to deformation in an Al-Mg-Mn alloy, Mater. Sci. Forum 495–497 (2005) 1049–1054.
[18] L.N. Brewer, D.P. Field, C.C. Merriman, Mapping and assessing plastic deformation using EBSD, in: A.J. Schwartz, M. Kumar, B.L. Adams, D.P. Field, D. (Eds.), Electron Backscatter Diffraction in Materials Science, Springer, Boston, 2009, pp. 251–261.
[19] J.K. Mackenzie, J.S. Bowles, The crystallography of martensite transformations. IV body-centred cubic to orthorhombic transformations, Acta Met. 5 (1957) 137–149.
[20] G. Aurelio, A. Fernández Guillermet, Assessment of the structural relations between the bcc and omega phases of Ti, Zr, Hf and other transition metals, Z. Met. 91 (2000) 35–42.
[21] A.R.G. Brown, D. Clark, J. Eastabrook, K.S. Jepson, The titanium-niobium system, Nature 201 (1964) 914–915.
[22] T. Yao, K. Du, H. Wang, Z. Huang, C. Li, L. Li, Y. Hao, R. Yang, H. Ye, In situ scanning and transmission electron microscopy investigation on plastic deformation in a metastable beta titanium alloy, Acta Mater. 133 (2017) 21–29.
[23] C. Li, J. Chen, Y.J. Ren, W. Li, J.J. He, J.H. Chen, Effect of solution heat treatment on the stress-induced martensite transformation in two new titanium alloys, J. Alloy. Compd. 641 (2015) 192–200.
[24] A. Bhattacharjee, V.K. Varma, S.V. Kamat, A.K. Gogia, S. Bhargava, Influence of β grain size on tensile behavior and ductile fracture toughness of titanium alloy Ti-10V–2Fe-3Al, Metall. Mater. Trans. A 37 (2006) 1423–1433.
[25] A. Paradkar, S.V. Kamat, The effect of strain rate on trigger stress for stress-induced martensitic transformation and yield strength in Ti-18Al-8Nb alloy, J. Alloy. Compd. 496 (2010) 178–182.
[26] S. Sadeghpour, S.M. Abbasi, M. Morakabati, Deformation-induced martensitic transformation in a new metastable β titanium alloy, J. Alloy. Comp. 650 (2015) 22–29.
[27] A. Paradkar, S.V. Kamat, A.K. Gogia, B.P. Kashyap, Effect of Al and Nb on the trigger stress for stress-induced martensitic transformation during tensile loading in Ti-Al-Nb alloys, Mater. Sci. Eng. A 487 (2008) 14–19.
[28] E.O. Hall, The deformation and ageing of mild steel: III discussion of results, Proc. Phys. Soc. Lond. B 64 (1951) 747.
[29] N.J. Petch, Cleavage of polycrystals, J. Iron Steel Inst. 174 (1653) 25.
[30] O. Bouaziz, S. Allain, C. Scott, Effect of grain and twin boundaries on the hardening mechanisms of twinning-induced plasticity steels, Scr. Mater. 58 (2008) 484–487.
[31] A. Devaraj, V.V. Joshi, A. Srivastava, S. Manandhar, V. Moxson, V.A. Duz, C. Lavender, A low-cost hierarchical nanostructured beta-titanium alloy with high strength, Nat. Commun. 7 (2016) 11176.
[32] C. Li, X. Mi, W. Ye, S. Hui, Y. Yu, W. Wang, A study on the microstructures and tensile properties of new beta high strength titanium alloy, J. Alloy. Compd. 550 (2013) 23–30.
[33] Y. Chen, Z. Du, S. Xiao, L. Xu, J. Tian, Effect of aging heat treatment on microstructure and tensile properties of a new β high strength titanium alloy, J. Alloy. Compd. 586 (2014) 588–592.